Multi-Stage Based Cross-Correlation Peak Detection for LTE Random Access Preambles

Felipe A. P. de Figueiredo, Fabbryccio A. C. M. Cardoso, José A. Bianco F., Rafael M. Vilela, Karlo G. Lenzi and Fabrício L. Figueiredo
DRC – Convergent Networks Department
CPqD – Research and Development Center
Campinas, SP - Brazil
{felipep, fcardoso, jbianco, rvilela, klenzi, fabricio}@cpqd.com.br

***Abstract* — Random Access is an important aspect of mobile systems where multiple users are always competing for resources. However, noise and interference imposes a significant problem to those systems causing them to falsely detect access requests. In consequence, unnecessary processing and air traffic are generated based upon these unreal request events. This paper presents a modified Cell-Average Constant False Alarm Rate (CA-CFAR) strategy applied to cross-correlation peak detection of random access CAZAC (Constant Amplitude and Zero-Autocorrelation) preambles in the presence of noise. Interference is also considered as uncorrelated noise, since the signals from other LTE cells are scrambled with different seeds (Physical Cell IDs). Simulation results indicate that the proposed method performs well even in the case of low SNR.**

Keywords: CA-CFAR, CAZAC, LTE, PRACH, Random Access, Signal Detection, Zadoff-Chu Sequence.

I. INTRODUCTION

The Random Access Channel (RACH) in Long Term Evolution (LTE) systems is mainly used for User Equipment (UE) to request resources from the Base Station (BS) [4]. In the Physical Random Access Channel (PRACH), cyclic-shifted versions of Zadoff-Chu (ZC) sequences are adopted as preambles. This adoption is based on the fact that ZC sequences present Constant Amplitude and Zero Auto-Correlation (CAZAC) properties [1-3], which turn them ideal to generate different preambles based on cyclic-shifted versions of the same root ZC sequence. Even when different root sequences are used, the cross-correlation exhibits high discrimination ability among the available preambles. A LTE UE can generate preambles by randomly selecting different root ZC sequences or by applying random cyclic shifts to the same ZC sequence [5, 6].

When detecting multiple random access requests from users in a mobile network, the task of a Random Access Detector is to decide whether only noise or requests-plus-noise are present. Interference from other cells is scrambled in LTE and will appear as uncorrelated noise. Therefore, this article only considers the effect of noise in the proposed method of detection.

A RACH detector typically determines if multiple accesses to the network are been requested based upon statistical computations of the cross-correlation function between the received PRACH signal and a root ZC sequence. The results from this statistical analysis are employed to calculate a threshold value that is then used to decide whether there are users requesting access or not. Correct selection of the threshold is very important once it determines the probability of false alarm, as well as the probability of detection [10].

It is of extreme necessity to determine a threshold value that produces both low alarm rate and good detection rate. However, the uncertainty of the noise variance is an important problem for the determination of a proper threshold. In the literature there are some well-known techniques for the reducing the noise effect [12]. One of them is the Cell-Averaging Constant False-Alarm Rate (CA-CFAR) method. CA-CFAR detectors have been proposed in [13] and [14] and consist of two steps: removing of the corrupted reference cells, also known as censoring, and the actual detection. In CA-CFAR detection, the detection threshold is the sum of the squared noise-only reference samples multiplied by a scaling factor [7]. In the case of wireless channels where the noise statistics are unknown, constant false alarm rate (CFAR) strategies can be used [15]. Therein the detection threshold is determined by using reference sets [15, 16].

In this paper, a modified version of the CA-CFAR method is presented and assessed. It is employed for detecting the presence of preamble sequences in the random access channel. The remainder of this work is organized as follows. Section II briefly describes the structure of the LTE signal. Section III introduces both the PRACH receiver structure adopted for user detection and the energy measurement the proposed method relies on. In Section IV, a modified version of a CA-CFAR detector is proposed. Results are presented and discussed in Section V. Finally, Section VI gives the conclusions.

II. LTE SIGNAL STRUCTURE

The LTE standard is based on Orthogonal Frequency Division Multiple Access (OFDMA) to reach high data rates and data volumes. High order modulation (up to 64QAM), large bandwidth (ranging from 1.25 MHz and up to 20 MHz) and Multiple Input Multiple Output (MIMO) transmission schemes in the downlink (up to 4x4) is also a part of the standard. The highest data rate is 75 Mbps in the uplink and with MIMO the rate can be as high as 300 Mbps in the downlink [8].

In order to achieve higher radio spectral efficiency, a multicarrier approach for multiple accesses is employed. OFDMA is used as the downlink modulation scheme and Single Carrier - Frequency Division Multiple Access (SC-FDMA) is used as the uplink scheme. LTE supports two duplex methods, namely, Frequency Division Duplex (FDD) and Time Division Duplex (TDD).

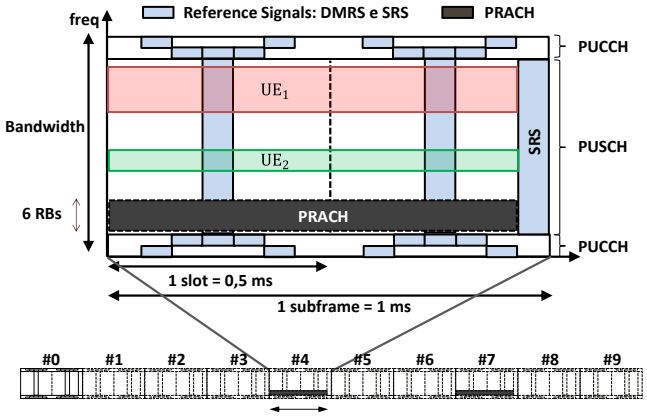

Fig. 1. LTE Generic Frame Structure for uplink LTE transmissions Systems.

The LTE standard also defines two frame structures: Type 1, used in FDD and Type 2, used in TDD [4]. This work will only focus on the FDD method and consequently, Type 1 frame structure.

A. *LTE Generic FDD Frame Structure*

Fig. 1 shows the LTE Generic Frame Structure for Uplink Frequency Domain Duplexing (FDD) [9]. As can be seen, LTE frames are 10 [ms] long. They are divided into 10 sub-frames with each sub-frame being 1.0 [ms] in duration. Each sub-frame is further split into two slots, each of 0.5 [ms]. Slots consist of either 6 or 7 ODFM symbols, depending on whether normal or extended cyclic prefix is employed.

The basic unit defined in the LTE system is called Resource Element (RE). A RE consists of one OFDM sub-carrier in one of the 6 or 7 OFDM symbols carried by a slot. In LTE, OFDM sub-carriers are spaced 15 KHz apart from each other. In the frequency domain, these sub-carriers, i.e., REs, are aggregated into groups of 12 consecutive sub-carriers in order to form Resource Blocks (RBs), which occupies a total bandwidth of 180 KHz in one slot duration. Resource Blocks, using pairs of slots (subframes), are employed to carry physical channels, *e.g.* PDSCH in the downlink and PUSCH in the uplink. PRACH is an exception because its time structure is design to fit a frame in the time domain and 6 RBs in the frequency domain. Furthermore, the PRACH subcarrier space is design to be 12 times less than downlink OFDMA and uplink SC-FDMA, corresponding to only 1.25 KHz.

As can be seen in Fig. 1, the PRACH is time and frequency-multiplexed with PUSCH and PUCCH. PRACH time-frequency resources are semi-statically allocated within the PUSCH region, and repeated periodically. The possibility of scheduling PUSCH transmissions within PRACH slots is left to the eNodeB's discretion [1, 10].

B. *Random Access Channel and Preamble Sequence Generation*

The Random Access Channel (RACH) is an uplink transport channel originated in the MAC layer, which is primarily used for initial network access and short message transmission, i.e. from UE to eNodeB (base station). The main purpose of the random access procedure is to obtain uplink time synchronization and to obtain access to the network [10]. The RACH channel is mapped into the PRACH channel.

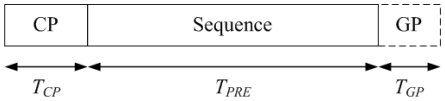

Fig. 2. Random Access Preamble.

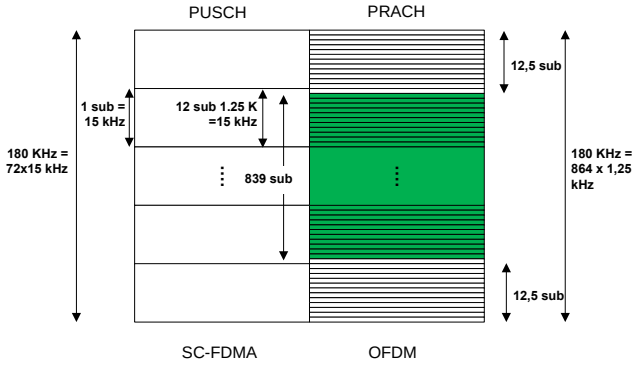

Fig. 3. PRACH preamble mapping onto allocated subcarriers [10].

The PRACH preamble, illustrated in Fig. 2, consists of three parts: a Cyclic Prefix (CP) with length T_{CP}, which is added to the preamble in order to effectively eliminate Inter-Symbol Interference (ISI), a signature or sequence part of length T_{PRE} and of a guard period T_{GP} which is an unused portion of time at the end of the preamble used for absorbing the propagation delay. The standard defines four different preamble formats for FDD operation [5]. Parameters T_{PRE}, T_{CP} and T_{GP} are set according to the chosen preamble format.

Prime-length ZC sequences are adopted as random access preambles in LTE systems due to its CAZAC properties, i.e., all points of the sequence lie on the unit circle and its auto-correlation is zero for all time shifts other than zero [1, 2]. These properties make ZC sequences very useful in channel estimation and time synchronization and also enable improved PRACH preamble detection performance [10].

The PRACH sequence, which is normally 800 [μs] long, is created by cyclically-shifting a ZC sequence of prime-length N_{ZC}, defined as [5]:

$$x_u(n) = \exp\left[-j\frac{\pi un(n+1)}{N_{ZC}}\right], \quad 0 \le n \le N_{ZC} - 1 \qquad (1)$$

where u is the ZC sequence index, n is the time index and the sequence length N_{ZC} = 839 for FDD systems [5]. This sequence length, N_{ZC}, corresponds to 69.91 Physical Uplink Shared Channel (PUSCH) subcarriers in each SC-FDMA symbol, and offers $72 - 69.91 = 2.09$ PUSCH subcarriers protection, which corresponds to one PUSCH subcarrier protection on each side of the preamble [5]. Note that the preamble is positioned centrally in the block of 864 available PRACH subcarriers, with 12.5 null subcarriers on each side.

The PRACH occupies a bandwidth of 1.08 MHz that is equivalent to 6 Resource Blocks (RB). Differently from other uplink channels, PRACH uses a subcarrier spacing of 1250 Hz for preamble formats 0 - 3 [5].

The preamble sequence, i.e., the N_{ZC} points generated by eq. (1), is specifically positioned at the center of the 1.08 MHz bandwidth so that there is a guard band of 15.625 KHz on each side of the preamble, which corresponds to 12.5 subcarriers. These guard bands are added to PRACH preamble edges in order to minimize interference from

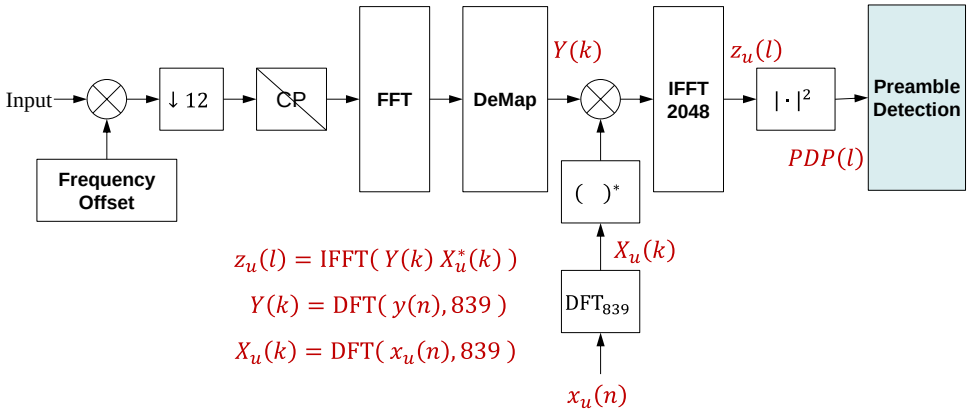

Fig. 4. PRACH preamble receiver structure.

PUSCH. Fig. 3 depicts the PRACH preamble mapping according to what was just exposed.

Therefore, the PRACH time-continuous preamble signal $s(t)$ can be written as follows [5]:

$$s(t) = \beta_{PRACH} \sum_{k=0}^{N_{ZC}-1} \sum_{n=0}^{N_{ZC}-1} x_{u,v}(n) e^{-j\frac{2\pi nk}{N_{ZC}}} \cdot e^{i2\pi\left(k+\varphi+K\left(k_0+\frac{1}{2}\right)\right)\Delta f_{RA}(t-T_{CP})}, 0 \le t < (T_{SEQ} + T_{CP}) \quad (2)$$

where β_{PRACH} is an amplitude scaling factor, k_0 controls the preamble location in the frequency domain, Δf and Δf_{RA} are subcarrier spacing for PUSCH and PRACH respectively and φ is a fixed offset determining the frequency-domain location of the PRACH preamble within the physical resource blocks.

From the uth root ZC sequence, random access preambles with zero correlation zones of length N_{CS} - 1 are defined by cyclic shifts according to:

$$x_{u,v}(n) = x_u\left((n + C_v) \bmod N_{ZC}\right) \quad (3)$$

where N_{CS} gives the fixed length of the cyclic shift, v is the sequence index and C_v is the cyclic shift applied to the root ZC sequence. All the possible values for these parameters are defined in [5].

C. Zadoff-Chu Sequences and Zero Correlation Zones

The main benefit of the CAZAC property is that it allows multiple orthogonal sequences to be generated from the same root ZC sequence. Indeed, if the periodic autocorrelation of a ZC sequence provides a single peak at the zero lag, the periodic correlation of the same sequence against its cyclic shifted replica provides a peak at lag N_{CS}, where N_{CS} is the number of samples of the cyclic shift and is defined in [5]. This creates a Zero-Correlation Zone (ZCZ) between the two sequences. As a result, as long as the ZCZ is dimensioned to cope with the largest possible expected time misalignment between them, the two sequences are orthogonal for all transmissions within this time misalignment i.e., the cyclic shift offset N_{CS} is dimensioned so that the ZCZ of the sequences guarantees the orthogonality of the PRACH sequences regardless of the delay spread and time uncertainty of the UEs [5, 10].

III. PRACH Receiver

In this section we present and explain the functionality of the PRACH receiver architecture adopted in this work. In the literature there are two approaches for PRACH receivers, the full frequency-domain one and the hybrid time/frequency domain one. The basic difference between the two approaches is the way each of them computes the sub-carriers bearing the preamble signal. The full frequency-domain approach easily extracts the PRACH sub-carriers by using a large IDFT, e.g., for a 20 MHz bandwidth system it would require 24576 points. This approach does not need any further processing in order to retrieve the transmitted cyclically shifted ZC sequences. However this large IDFT sizes leads to cumbersome implementations [10].

In order to reduce the complexity, especially for the number of multiplications performed at the preamble detector at eNodeB, we adopt the hybrid time/frequency domain approach, which results in more practical implementations [10]. Fig. 4 depicts the PRACH receiver architecture adopted in this paper.

The received signal is first pre-processed in time domain, then transformed to the frequency domain by the FFT block and multiplied with the Fourier transformed RACH sequence. The cross-correlation is obtained by transforming the multiplication result back to time domain, which is performed by the IFFT and zero-padding blocks. Fig. 4 describes the main components of the RACH preamble detector, using a DFT-based (frequency-domain) SC-FDMA receiver [11].

The first block in Fig. 4 represents a down-converter, which shifts the PRACH pass-band signal to base-band. After down-converting the signal, a linear filter is applied in order to avoid aliasing after decimation. The result of the decimation block is fed into the CP removal block. After removing the Cyclic Prefix, the FFT engine transforms the SC-FDMA symbols from time domain into frequency domain. The sub-carrier de-mapping block extracts the RACH preamble sequence from the output of the FFT engine. The result of sub-carrier de-mapping is multiplied by the root ZC sequence and then fed into a zero-padding block. Finally, the IFFT engine transforms the cross-correlation result from frequency domain into time domain. All samples coming out of the IFFT block have their square-modulus calculated producing the Power Delay Profile (*PDP*) samples. For further information on this receiver architecture, refer to [10].

The preamble detection block employs the *PDP* samples to estimate noise power, set the detection threshold and then decide whether a preamble is present or not. As output of the detection process this block sends to the MAC layer the Signatures, C_v and Channel Propagation Delay, N_{CH} (also referred as Time Advance, *TA*) estimates of all detected preambles.

A. Power Delay Profile Computation

The LTE PRACH receiver benefits from the PRACH format and CAZAC properties as described in [11] by computing the PRACH Power Delay Profile (*PDP*) through a frequency-domain periodic correlation. The *PDP* of the received sequence is given by:

$$PDP(l) = |z_u(l)|^2 = \left| \sum_{n=0}^{N_{ZC}-1} y(n) x_u^*[(n+l)_{N_{ZC}}] \right|^2 \quad (4)$$

where $z_u(l)$ is the discrete periodic correlation function at time lag l between the received sequence $y(n)$ and the locally generated root ZC sequence $x_u(n)$ where $(.)^*$ denotes the complex conjugate. The length of both sequences is N_{ZC}. It is worth noticing that by making use of the properties of the DFT, $z_u(l)$ can efficiently be computed in the frequency domain.

The fact that different PRACH signatures are generated by applying randomly selected cyclic shifts to a common root ZC sequence means that the frequency-domain *PDP* computation of a root ZC sequence provides in a one-shot the concatenated PDPs of all signatures derived from the same root ZC sequence [10]. Therefore, the signature detection process consists in searching the *PDP* samples for peaks above a given detection threshold over a search window which corresponds to the cell size. Fig. 5 illustrates the result of the computation of the *PDP* when two different users transmit two simultaneous preambles. As depicted in the figure, by searching the *PDP* for peaks above a given threshold it is possible to estimate both the preamble ID and the propagation delay of each user.

Due to the unique correlation properties of ZC sequences, the preamble ID is indicated by the peak position information and its cyclic shift value, C_v. If the preamble is received with a certain amount of propagation delay, the peak position is affected not only by C_v but also by the amount of propagation delay. As illustrated in Fig. 5, the position of a peak is delayed in temporal domain by the amount of propagation delay. According to this, the preamble detection algorithm can estimate the ID and its propagation delay exactly if the quantity of propagation delay in temporal domain is less than the cyclic shift offset, N_{CS} [10, 20].

IV. Proposed Multi-Stage Preamble Detection Algorithm

The energy measurement and the collected data processing are performed in baseband by a device with the architecture depicted in Fig. 4. The detection method proposed here is carried out in three stages making use of the *PDP* samples.

The preamble detection procedure consists basically of hypothesis tests following the Neyman&Pearson lemma

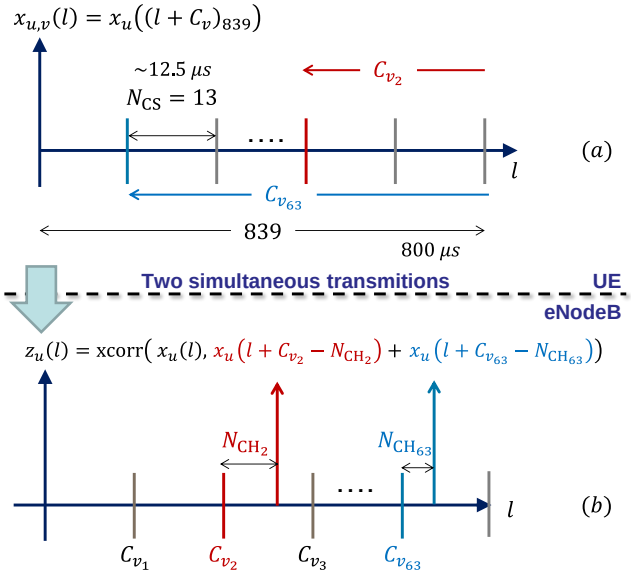

Fig. 5. Cross-correlation result (b) is presented when two simultaneous cyclic-shifted ZC versions are transmitted as preambles. Figure (a) is simplified to show only the cyclic shifts applied to the root ZC sequence $x_u(l)$. Figure (b) is also simplified, showing only the cross-correlation peaks.

[17]. This lemma establishes that detectors based on likelihood ratio tests:

$$\frac{PDP_{H_1}}{PDP_{H_0}} > \gamma, \quad (5)$$

where the hypothesis H_0 is rejected in favor of H_1 when the desired signal (preamble) is present, is optimum when the cumulative distribution function (CDF) of this ratio given the hypothesis H_0 is known, so that it is possible to calculate the threshold γ that satisfies:

$$P\left\{\frac{PDP_{H_1}}{PDP_{H_0}} > \gamma \mid H_0\right\} = P_{FR} \quad (6)$$

for a given false rejection probability P_{FR}. Typically, the derivation of this function assumes the knowledge of the probability distribution function of both random variables PDP_{H_1} and PDP_{H_0}.

The method proposed in this paper is composed of three stages. The first stage is used to identify *PDP* samples that can be considered as containing only the presence of noise, i.e., energy samples, which better represent the hypothesis H_0. These noisy-only samples are used to calculate an energy value employed as reference, PDP_{ref}.

The reference value, PDP_{ref} is used in the second stage to calculate the decision threshold γ of the hypothesis test.

The third stage makes use of both the decision threshold γ and the reference value, PDP_{ref}, to test each one of the *PDP* samples. This procedure makes it possible to reliably decide if there is signal being transmitted on the PRACH channel.

A. Censoring Algorithm and Calculation of the Reference Noise Energy

The censoring algorithm adopted in this paper is known as Forward Consecutive Mean Excision (FCME) [16]. The basic principle of the algorithm consists in sorting the *PDP* samples in ascending order of energy.

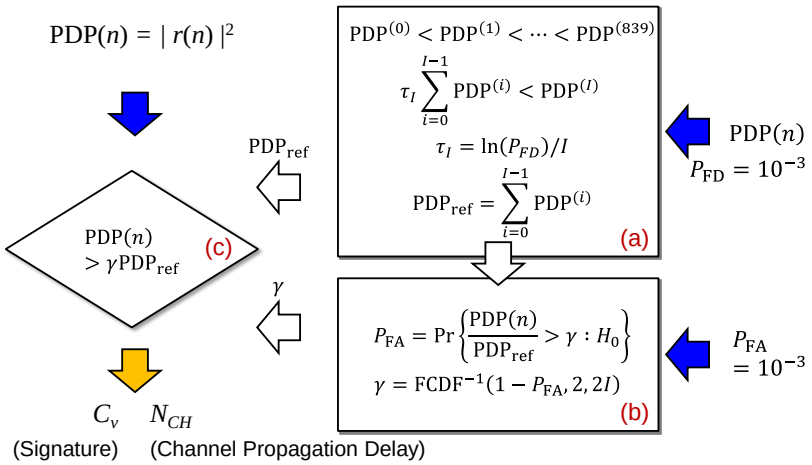

Fig. 6. Summary of the proposed multi-stage detection algorithm: (a) Stage 1 is used to calculate PDP_{ref}; (b) Stage 2 is used to calculate threshold γ; (c) last stage uses Statistical test to calculate C_v and N_{CH}.

$$\{PDP(i) \mid i = 0,1,\dots,N_{ZC}-1\} \tag{7}$$

which results in the ordered set:

$$\left\{PDP^{(i)} \middle| \, i = 0,1,\dots,N_{ZC}-1\right\} \tag{8}$$

where,

$$PDP^{(0)} < PDP^{(1)} < PDP^{(2)} < \cdots < PDP^{(N_{ZC}-1)} \tag{9}$$

Then it discards all samples with energy greater than $PDP^{(I)}$, such that:

$$PDP^{(I)} > \tau_I \sum_{i=0}^{I-1} PDP^{(i)} \tag{10}$$

where τ_I is the censoring scaling factor at the Ith step.

The algorithm used to search for $PDP^{(I)}$ is performed iteratively, being necessary to calculate the censoring scaling factor τ_I for each iteration. The scale factor calculation is done under the initial assumption that $PDP^{(I)}$ is a PDP sample that only contains noise, i.e., free of the presence of signal. Under this assumption, the probability that this test is true corresponds to a probability of false disposal P_{FD} given by

$$P_{FD} = P\left\{PDP^{(I)} > \tau_I \sum_{i=0}^{I-1} PDP^{(i)} \mid H_0\right\} \tag{11}$$

where P_{FD} is a predefined constant. Each iteration starts with I equal to the size of the smallest assumed clean set of PDP samples. The larger the smallest assumed clean set is the better censoring works. However, if the assumed clean set is too large, the probability that corrupted samples will be part of the initial clean set increases. The iteration procedure continues until the test in eq. (10) is true for some value of I or all the reference samples are decided to be signal-free [15].

As the quadrature components of the correlation signal $z_u(l)$ present Gaussian distribution with zero mean and variance equal to $N_{ZC}\sigma^2/2$, the PDP samples, consequently, present a non-central Chi-squared distribution with 2 degrees of freedom and mean given by [10]

$$E\left[PDP^{(i)}\right] = N_{ZC}\sigma^2 \tag{12}$$

Equivalently, each PDP sample presents an exponential distribution that is a special case of the Chi-square distribution. Furthermore, since:

$$\sum_{i=0}^{I-1} PDP^{(i)} \simeq I \, \mathrm{E}\left[PDP^{(i)}\right] \tag{13}$$

Then the equation for the probability of false disposal P_{FD} can be approximated by:

$$P_{FD} = P\left\{PDP^{(I)} > \tau_I \, I \, N_{ZC}\sigma^2\right\} \tag{14}$$

This approach becomes better as the set of reference samples I increases. Therefore, the probability of false disposal P_{FD} can be approximated by:

$$P_{FD} = e^{-\tau_I \, I} \tag{15}$$

The probability of false disposal P_{FD} can be viewed as the desired clean sample rejection rate. Samples that have value above the threshold are discarded and then the new set consists of the remaining samples. The output of the censoring (disposal) stage is then defined by the total energy of the noise reference samples, which is then calculated by:

$$PDP_{ref} = \sum_{i=0}^{I-1} PDP^{(i)} \tag{16}$$

and also by the number of PDP samples I employed to calculate PDP_{ref}.

B. Threshold Calculation

After defining the set of reference samples containing only noise, the next stage consists in testing each PDP sample against PDP_{ref}, which is performed through evaluation of the following hypothesis test:

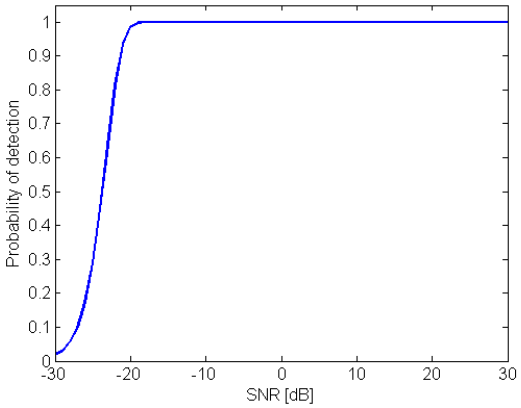

Fig. 7. Simulated detection probability.

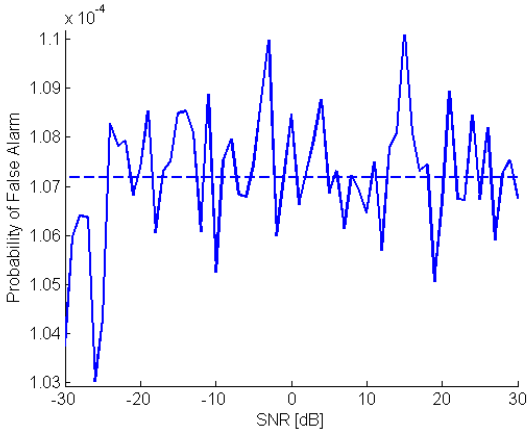

Fig. 8. Simulated false alarm probability.

$$PDP(l) \geq \gamma\, PDP_{ref}, \quad \text{for} \quad l = 0, 1, \ldots, N_{ZC} - 1 \tag{17}$$

where γ is the detection threshold which is determined by the decision method employed. Herein the Cell Averaging (CA) method is employed to calculate the detection threshold γ [15].

The detection threshold γ is calculated under the hypothesis of signal absence, i.e., the reference samples contain only noise, for a given probability of false alarm P_{FA} defined as:

$$P_{FA} = P\left\{\frac{PDP(l)}{PDP_{ref}} > \gamma \mid H_0\right\} \tag{18}$$

Once it is assumed that the quadrature components of the PDP have Gaussian distribution, therefore in consequence, the energy measures $PDP(l)$ and PDP_{ref} present non-central Chi-square distribution with 2 (exponential distribution) and $2I$ degrees of freedom, respectively. Given that the ratio between two Chi-square distributions results in a *Fisher* distribution whose cumulative distribution function is given by:

$$FCDF(\gamma) = 1 - P\left\{\frac{PDP(l)/2}{PDP_{ref}/2I} > I\,\gamma\right\} \tag{19}$$

then the detection threshold γ is calculated by

$$\gamma = FCDF^{-1}(1 - P_{FA}, 2, 2I)/\, I \tag{20}$$

where $FCDF$ is the Fisher Cumulative Distribution Function.

C. Preamble Detection Procedure

The preamble detection procedure consists of searching for *PDP* peaks above the detection threshold, γ over all ZCZs. In other words, the test given by eq. (17) is evaluated against the samples within all ZCZs. If the test is true, signal(s)-plus noise hypothesis H_1 is chosen, i.e., a user is requesting access. Otherwise, the noise-only hypothesis H_0 is decided to be true. Fig. 6 illustrates the proposed multi-stage preamble detection method.

The length of the ZCZs is defined by the N_{CS} parameter and it corresponds to the cell size. Therefore, the time misalignment between UE and eNodeB can be measured in terms of the number of *PDP* time lags between the detected peak and the beginning of a ZCZ. This measurement provides both the transmitted preamble, C_v and the time advance, TA that must be applied to the UE in order to align its subsequent uplink transmissions. Both values are reported back to the MAC layer.

V. Numerical Results

The threshold given by the method proposed here is found via computer simulations. The number of Monte Carlo runs was greater than 10^5 iterations. The ideal AWGN channel is assumed. During the simulations, a user is said present when the energy of a given *PDP* sample is greater than the estimated threshold. In this paper, the initial set size for the censoring stage is made equal to 25% of N_{ZC}, which is the reference set.

For the results presented here, the probability of false alarm P_{FA} is made equal to 10^{-4} and the probability of false disposal P_{FD} is made equal to 10^{-3} and therefore, evaluating equation (14) results that the value for $\tau_I\, I = T_{CME}$ is 6.9078.

Fig. 7 shows the simulated detection probability for one signature generated from one ZC root sequence when the SNR varies from -30 [dB] up to 30 [dB]. It can be noticed that for SNR values greater than -20 [dB], the probability of correct detection is 1, i.e., the presence of a preamble is always detected.

Fig. 8 depicts the corresponding false alarm probability when the SNR varies from -30 [dB] up to 30 [dB]. It can be noticed that P_{FA} varies from approximately 1.03 x 10^{-4} up to 1.1 x 10^{-4}, showing that the method keeps P_{FA} close the value set previously for that parameter.

A comparison between the desired P_{FA}, which is varied from 1 x 10^{-5} up to 1 x 10^{-4}, and the value achieved by the proposed method is presented in Fig. 9. As can be noticed, the achieved P_{FA} value stays rather close to the desired one.

Fig. 10 shows P_D versus P_{FA} (ROC plot). In that figure P_{FA} is also varied from 1 x 10^{-5} up to 1 x 10^{-4} with SNR equal to 0 [dB]. It shows an ideal ROC curve where the presence of a user is always detected independently of the value of PFA.

The proposed method achieves better performance than the methods presented in [18] and [19], where the probabilities of false alarm, P_{FA}, are 5 x 10^{-3} and 10^{-4} respectively. The only drawback presented by the method is its moderate to high computational complexity due to the sorting procedure, to the iterative search for a reference set containing only noise and to the test procedure which checks

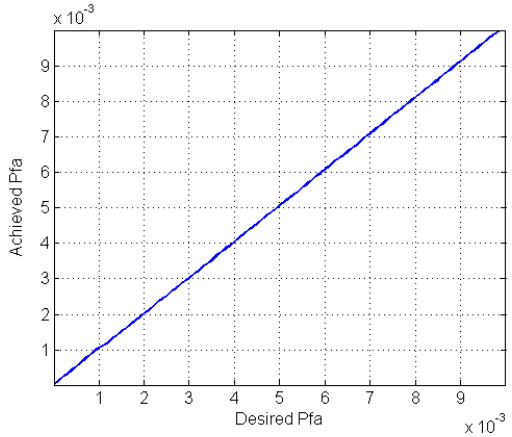

Fig. 9. Comparison between the desired P_{FA} and the actually achieved value, where SNR = 0 [dB].

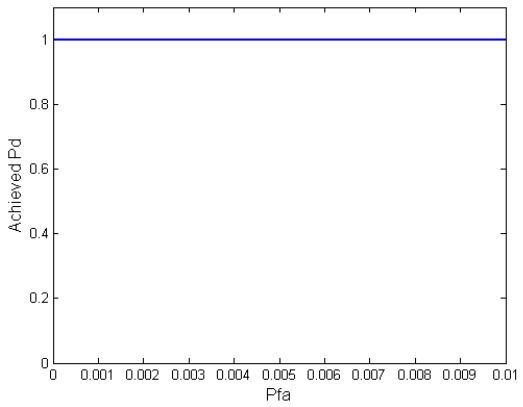

Fig. 10. ROC plot showing PD versus PFA with SNR = 0 [dB].

each one of the *PDP* samples for the presence of the desired signal. This drawback increases the time the method takes to detect the presence of a user and may impose a constraint to both the number of users it can simultaneously detect and the cell size depending on the architecture the method is implemented.

VI. CONCLUSION

A multi-stage preamble detection algorithm based on a CA-CFAR method was proposed in this paper. Its main goal is to detect CAZAC sequences that are sent by UEs in order to request the allocation of resources. The numerical results showed that the modified iterative CA-CFAR method proposed here could detect the presence of a user even in the case of SNR as low as -17 [dB]. Also, as the results presented here show that the proposed method does well even in low SNR environments it could be suitable for cognitive radios.

Future work will concentrate on investigations to improve the performance and decrease the computational complexity presented by the proposed method allowing it to be easily implemented in any architecture. Additionally, the influence of the use of antenna diversity over the performance of the method will be assessed as well.

ACKNOWLEDGMENT

This work was supported by Funttel project "RASFA-4G" at CPqD Telecom and IT Solutions.

REFERENCES

[1] R. L. Frank, S. A. Zadoff and R. Heimiller, "Phase shift pulse codes with good periodic correlation properties," IRE Transactions on Information Theory, Vol 7, pp.254-257, October 1961.

[2] David C. Chu, "Polyphase codes with good periodic correlation properties" IEEE Transactions on Information Theory, pp. 531-532, July 1972.

[3] Mansour, M. M., "Optimized architecture for computing Zadoff-Chu sequences with application to LTE," GLOBECOM 2009. IEEE, Nov. 30 2009-Dec. 4, pp. 1-6, 2009.

[4] 3GPP TS 36.213, "Physical layer procedures (Release 8)", September 2009.

[5] 3GPP TS 36.211, "Physical Channels and Modulation (Release 8)", September 2009.

[6] 3GPP TSG RAN WG1 Meeting #44bis, R1-060998, Ericsson, "E-UTRA Random Access Preamble Design", March 2006.

[7] P. P. Gandhi and S. A. Kassam, "Analysis of CFAR processors in nonhomogeneous background," IEEE Trans. Aerosp. Electron. Syst., vol. 24, no. 4, pp. 427–445, Jul. 1988.

[8] 3GPP, "LTE Overview", http://www.3gpp.org/LTE, accessed on November 1, 2012.

[9] J. Zyren, "Overview of the 3GPP Long Term Evolution Physical Layer", 2007.

[10] Stefania Sesia, Issam Toufik and Matthew Baker, "LTE - The UMTS Long Term Evolution: From Theory to Practice", John Wiley & Sons, 2011.

[11] 3GPP TSG RAN WG1 Meeting #46bis, R1-062630, Texas Instruments, "Non-synchronized Random Access structure for E-UTRA", October 2006.

[12] T. Yucek, H. Arslan, "A survey of spectrum sensing algorithms for cognitive radio applications", IEEE Communications Surveys & Tutorials, v.11 n.1, p.116-130, January 2009.

[13] M. Barkat, S. D. Himonas, and P. K. Varshney, "CFAR detection probabilities for multiple target situations," in *Proc. Inst. Elect. Eng.*, vol. 136, Oct. 1989, pp. 194–209.

[14] S. D. Himonas and M. Barkat, "Automatic censored CFAR detection for nonhomogeneous environments," *IEEE Trans. Aerosp. Electron. Syst.*, vol. 28, no. 1, pp. 286–304, Jan. 1992.

[15] Janne J. Lehtomäki, Markku Juntti and Harri Saarnisaari, "CFAR Strategies for Channelized Radiometer", IEEE Signal Processing Letters, Vol. 12, No. 1, January, 2005.

[16] Janne J. Lehtomäki, Johanna Vartiainen, Markku Juntti and Harri Saarnisaari, "Spectrum sensing with forward methods," in Proc. IEEE Military Commun. Conf., pp. 1–7, Washington, D.C., USA, Oct. 2006.

[17] J. Neyman and E. S. Pearson, "On the problem of the most efficient tests of statistical hypotheses", Philosophical Transactions of the Royal Society of London, Series A. 231: 289–337, 1933.

[18] Marjan Mazrooei Sebdani and M. Javad Omidi, "Detection of an LTE Signal Based on Constant False Alarm Rate Methods and Constant Amplitude Zero Autocorrelation Sequence", International Conference on Intelligent and Advanced Systems (ICIAS), Kuala Lumpur, Malaysia, Jun. 2010.

[19] Asier Freire-Irigoyen, Rodolfo Torrea-Duran, Sofie Pollin, Min Li, Eduardo Lopez and Liesbet Van der Perre, "Energy Efficient PRACH Detector Algorithm in SDR for LTE Femtocells", 18th IEEE Symposium on Communications and Vehicular Technology (SCVT), Nov. 2011.

[20] Sungbong Kim, Kyunghwan Joo and Yonghoon Lim, "A delay-robust random access preamble detection algorithm for LTE system", IEEE Radio and Wireless Symposium (RWS), January 2012.